DIGITAL PRESERVATION OF *LABU SAYONG*: A COMPARATIVE STUDY OF HIGHER-ORDER GT-BÉZIER CURVES

Nurul Atifah Norisham, *Noor Khairiah Razali

Faculty of Computer and Mathematical Sciences, Universiti Teknologi MARA Cawangan Terengganu Kampus Kuala Terengganu, Terengganu, Malaysia

***Corresponding Author**

DOI: https://doi.org/10.47772/IJRISS.2026.100500471

Received: 05 May 2026; Accepted: 11 May 2026; Published: 04 June 2026

ABSTRACT

This paper explores the modeling of the *Labu Sayong*, a traditional Malaysian pottery form, using higher-order Generalized Trigonometric (GT) Bézier curves. The research compares Cubic (m = 3) and Quartic (m = 4) curves through the rotational sweep surface method. Evaluation metrics include Root Mean Square Error (RMSE) for geometric accuracy, CPU processing time for computational efficiency, volumetric calculations for functional preservation and curvature profiles for smoothness. Data was extracted from a symmetrical reference image and discretized into 24 distinct segments, utilizing 72 control points for the Cubic model and 96 for the Quartic model. Results indicate that the Cubic GT-Bézier curve achieves superior accuracy with a lower average RMSE of 1.33759 and a faster average computation time of 96.78 seconds. Furthermore, curvature assessment confirms that the Cubic formulation maintains a stable organic flow without the localized ripple distortions observed in the Quartic model. These findings conclude that higher-order curves do not necessarily guarantee superior reconstruction, with the Cubic curve providing the optimal balance between mathematical precision and computational efficiency for the digital preservation of axially symmetric cultural artifacts.

Keywords: GT-Bézier curves, Cubic curve, Quartic curve, Sweep surface method, 3D geometric modeling, *Labu Sayong*.

INTRODUCTION

Computer-Aided Geometric Design (CAGD) has long been a substantial part of such disciplines as computer graphics, industrial design and engineering in that it provides the mathematical framework to allow the representation and manipulation of geometric shapes in both two and three dimensional space. One of its tools, the classical Bézier curve, is still popular due to its simplicity in structure (control points), smoothness and compatibility with modeling software. Nevertheless, a local lack of flexibility is one of the key disadvantages. The shape of a Bézier curve must be changed by changing the location of the control points, which in the case of detailed or complex surfaces can be cumbersome and inefficient.

There have been many extensions created in the past concerning the Bézier curve to increase its flexibility. Generalized forms and rational, trigonometric, and other forms have been made that have more control yet maintain the important geometric properties. One of the recent developments is the Generalized Trigonometric (GT) Bézier curve by Maqsood et al. (2020). This brings in two shape parameters, that allow the local change of tension in the curve without adjusting the control polygon. The formulation has the same property as the curve, the partition of unity, the interpolation of the endpoint, and the affine invariance, but with a better design flexibility of curves and surfaces.

Labu Sayong has been picked as the case study in this current research work. The Malay water vessel, which is traditionally pleasing in shape, has a nice curvy proportions in addition to rotational symmetry. Despite the fact that numerous researchers have already discussed the cultural and aesthetic aspects of *Labu Sayong* (Arifin, 2015; Hamdzun Haron et al., 2018; Abd Aziz and Samsudin, 2025), mathematical reconstruction with the help of the CAGD, has not been widely studied. The majority of the models that have been developed so far assume classical Bézier curves or direct drawing in CAD, with little consideration given to how these new curve formulations can affect the modeling accuracy or computational efficiency (Razali et al., 2019).

An overview of the literature shows that the GT Bézier curves have very good shape control, but the performance of the various curve orders in three-dimensional (3D) reconstructions is not yet systematically studied. The connection between the order of a curve, precision and computational efficiency is still unclear. Equally, how the GT Bézier curves and the rotational sweep surface technique can be integrated into modeling cultural artifacts has rarely been mentioned. This indicates a lack of further research into the role of higher-order formulations on model fidelity and processing cost in applications of CAGD.

This paper, then, compares the performance of Cubic (m = 3) and Quartic (m = 4) GT Bézier curves in reconstructing Labu Sayong using the rotational sweep surface technique. The performance was measures based on Root Mean Square Error (RMSE) for geometric accuracy, CPU processing time for computational efficiency, volumetric calculations for functional preservation and curvature profiles for smoothness, to determine the effect of the order of the curve on the trade-off between accuracy and computational demand. The current research will introduce new information about the GT Bézier curves in the reconstruction of the cultural heritage and expand the information related to the curve-based modeling in the context of CAGD.

Related Works

Bézier curves and their extensions are also part and parcel of CAGD since they represent rigor in mathematical definition, natural smoothness, and a vast array of applications in geometric modeling and the visualization processes (Farin, 2002; Sederberg, 2012). However, classical Bézier curves have poor local control in that any change in the curve requires global updating the control points. To overcome the drawbacks, some refined formulations were proposed, e.g., rational, trigonometric and generalized Bézier curves, each of which introduced shape parameters to augment the flexibility of classical curves but retained their key geometric characteristics. The recent advancements in this respect include the introduction of the GT-Bézier curve, which was introduced by Maqsood et al. (2020), and which allows two independent shape parameters to be used in adjusting the curve tension without interfering with the control polygon. Basically this formulation retains all the primary properties of Bézier curves, including endpoint interpolation, convex hull containment and affine invariance, whilst providing locally deformable curves that are of superior smoothness. Up to this point, GT-Bézier curves have demonstrated their potential merits in engineering, and aesthetic modeling and analysis, as it provides an effective trade-off between geometric accuracy and computational efficiency.

Continuous Bézier curves of higher order have further served to illustrate the desirability of continuity and fairness of complex modeling tasks. Qin et al. (2016) studied the G1 continuity of quartic C-Bézier curves, which established mathematical conditions of smooth transitions in the shape of surface patches. Hu, Ji, and Guo (2014) developed multiple shape parameter quartic generalized Bézier surfaces that enhanced continuity across surface patches. Equally, Sun, Qiao, and Li (2019) proposed the subdivision of quartic Bézier curves to enhance the stability of refinement and Yu, Li, and Ji (2024) were interested in the self-intersectioning nature of cubic Bézier curves to ensure geometrical accuracy. All these studies together highlight the fact that, despite higher-order Bézier curves being more flexible, they are also more sensitive to control parameters and more complex to compute.

The sweep surface method, being one of the preferred methods, in the process of generating smooth and symmetric 3D geometries, has been widely used to construct smooth and symmetric 3D geometries by rotating a profile curve around an axis. In essence, this method provides a good mechanism of generating continuous surfaces with works like those presented by Meng et al. (2021), who developed the variational framework of computing geodesic paths on sweep surfaces, and by Mahmoud, Soliman, and Mohamed (2023), who introduced the Isotropic Bézier Sweeping Surface model where the Bishop frame is used to minimize twisting and deformation. Equally, the concept of parametric curves design too, holds considerable importance in the engineering practice. To be more precise, as Zhang, Yang, and Li (2009) demonstrated, the geometric parameters of curves may directly impact the aerodynamic and hydraulic performances, therefore, once again, mathematical modeling can be assigned an important role in the industrial and cultural life.

With these advances, however, comparative studies that take into account the various orders of GT-Bézier curves example cubic, quartic orders and others. In the 3D reconstruction algorithms are still lacking. Moreover, there are very few studies that have matched GT-Bézier representations with techniques used to generate sweep surfaces so as to evaluate the performance as far as geometric accuracy and computational efficiency are concerned. The majority of the prior modeling work is on a basis of Bézier or NURBS representations (polynomials), which, although efficient, do not demonstrate the same level of shape flexibility of generalized trigonometric representations. In the area of reconstruction of cultural heritage, 3D modeling is a topical tool in the protection and recording of traditional objects. On the one hand, as has been mentioned above, such objects as *Labu Sayong* have been researched due to their historical and aesthetic value. Conversely, it remains at quite a rudimentary level as compared to mathematical reconstruction with state-of-the-art CAGD techniques.

Therefore, the research work is guided to fill these gaps by the integrating of the formulations of the GT-Bézier curves with a rotational sweep surface approach of the modeling of traditional *Labu Sayong*. In particular, it compares cubic and quartic GT-Bézier curves according to their geometric fidelity, computational efficiency, and geometric smoothness. By so doing, the current study does not only support the development of more efficient CAGD modeling techniques, but also supports the development of digital preservation of cultural artefacts using mathematically based 3D reconstruction techniques.

METHODOLOGY

This section describes mathematical as well as the computational methodologies adopted for the construction and analysis of *Labu Sayong's* 3D geometric model. The workflow takes several important steps: starting with the generation of two-dimensional (2D) profile curves by fitting Cubic and Quartic GT-Bézier curves and finishing with the creation of a 3D model by applying the rotational sweep surface technique. After this, the model geometrical fidelity is quantitatively evaluated by the Root Mean Square Error (RMSE) for geometric accuracy between the reconstructed curves and the reference data profiles and computational performance by the CPU execution time, curvature profiles for smoothness, and volumetric calculations for functional preservation. It is based on the combination of the geometric accuracy and computing efficiency with respect to CAGD modeling and reconstruction research.

Mathematical Framework Of Gt-Bézier Curves

The GT-Bézier curve is an extension of the classical definition of the Bézier curve, adding two shape parameters, α and β, that are independent of each other. This leads to a much broader latitude in modifying curve tension and form without changing main primary geometric properties of Bézier curves. An example is that endpoint interpolation, convex hull containment, affine invariance, and parametric continuity are also observed in GT-Bézier curves, and meet mathematical robustness and practical suitability in a wide variety of applications in geometric design and modeling.

A GT-Bézier curve of degree m is defined as, (Maqsood et al., 2020):

Definition 1: Degree 2 GT-Basis Functions

GT-basis functions are formulated using a recurrence technique and incorporate two shape parameters $[\alpha, \beta]$.

For $(-1 \leq \alpha, \beta \leq 1)$ and $(0 \leq z \leq 1)$, the degree 2 GT-basis functions defined as:

$$\begin{cases} w_{0,2}(z) = \left(1 - sin\left(\frac{\pi}{2}z\right)\right)\left(1 - \alpha\, sin\left(\frac{\pi}{2}z\right)\right) \\ w_{1,2}(z) = \left(1 - w_{0,2}(z) - w_{2,2}(z)\right) \\ w_{2,2}(z) = \left(1 - co\,s\left(\frac{\pi}{2}z\right)\right)\left(1 - \beta\, cos\left(\frac{\pi}{2}z\right)\right) \end{cases} \tag{1}$$

ISSN No. 2454-6186 | DOI: 10.47772/IJRISS | Volume X Issue V May 2026

The recursive relationship for higher-degree GT-basis functions is:

$$w_{i,m}(z) = \left(1 - sin\left(\frac{\pi}{2}z\right)\right) w_{i,m-1}(z) + sin\left(\frac{\pi}{2}z\right) w_{i-1,m-1}(z) \tag{2}$$

From equation (2) shows that is GT-basis function for m (order 3 and above). When, $> m$, the function $w_{i,m}(z) = 0$.

Definition 3: Recursive Relationship for Higher-Degree Functions

For any control points $P_i \in R^2$ or $R^3 (i = 0,1,2,..,m)$ and shape parameter α, β, and $w_{i,m}(z)$ are GT-basis function at equation (2). The GT-Bezier curve can be constructed as

$$S(z) = \sum_{i=0}^{m} P_i w_{i,m}(z), \tag{3}$$

Formulation of Cubic (m=3) and Quartic (m=4) Models

The Cubic and Quartic cases used in this study are represented respectively as:

The Basis function of Cubic (m=3)

$$\begin{cases} w_{0,3}(z) = \left(1 - sin\left(\frac{\pi}{2}z\right)\right) w_{0,2}(z), \\ w_{1,3}(z) = sin\left(\frac{\pi}{2}z\right) w_{0,2}(z) + \left(1 - sin\left(\frac{\pi}{2}z\right)\right) w_{1,2}(z), \\ w_{2,3}(z) = \left(1 - sin\left(\frac{\pi}{2}z\right)\right) w_{2,2}(z) + sin\left(\frac{\pi}{2}z\right) w_{1,2}(z), \\ w_{3,3}(z) = sin\left(\frac{\pi}{2}z\right) w_{2,2}(z) \end{cases} \tag{4}$$

The curves of Cubic GT-Bezier as follows:

$$S(z) = \sum_{i=0}^{m=3} P_i w_{i,3}(z), \tag{5}$$

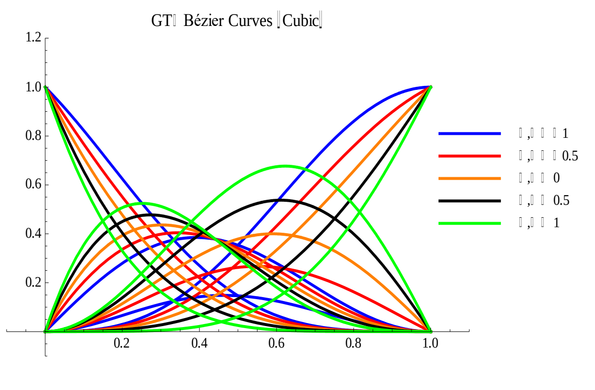

Figure 1: The Cubic GT-basis functions

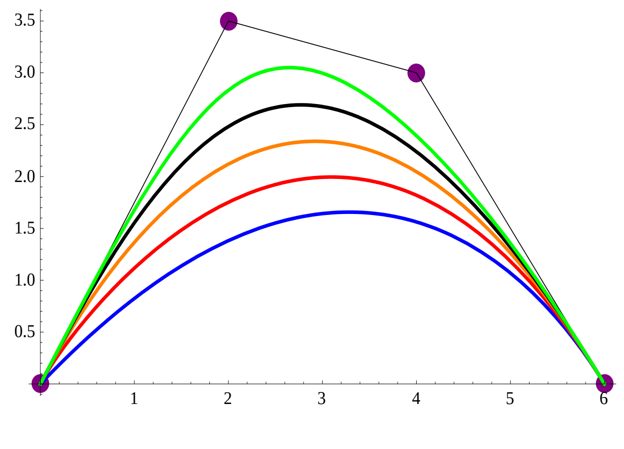

Figure 2: The Cubic GT-basis curves

Figure 1 and 2, shows all the graphs of Cubic GT-basis functions and curves. There are five shape parameters manipulated by alpha and beta [α, β], represented by the following colours: thick blue for [-1, -1], dotted red for [-0.5, -0.5], thick orange for [0, 0], dashed black for [0.5, 0.5], and thick green for [1, 1].

The Basis function of Quartic (m=4)

$$\begin{cases} w_{0,4}(z) = \left(1 - sin\left(\frac{\pi}{2}z\right)\right)^2 w_{0,2}(z), \\ w_{1,4}(z) = \left(1 - sin\left(\frac{\pi}{2}z\right)\right)\left(2\, sin\left(\frac{\pi}{2}z\right) w_{0,2}(z) + \left(1 - sin\left(\frac{\pi}{2}z\right)\right) w_{1,2}(z)\right), \\ w_{2,4}(z) = sin\left(\frac{\pi}{2}z\right)^2 w_{0,2}(z) + \left(1 - sin\left(\frac{\pi}{2}z\right)\right)^2 w_{2,2}(z) + 2\, sin\left(\frac{\pi}{2}z\right)\left(1 - sin\left(\frac{\pi}{2}z\right)\right) w_{1,2}(z), \\ w_{3,4}(z) = sin\left(\frac{\pi}{2}z\right)\left(2\left(1 - sin\left(\frac{\pi}{2}z\right)\right) w_{2,2}(z)\right) + sin\left(\frac{\pi}{2}z\right) w_{1,2}(z), \\ w_{4,4}(z) = sin\left(\frac{\pi}{2}z\right)^2 w_{2,2}(z) \end{cases} \quad (6)$$

The curves of Quartic GT-Bezier as follows:

$$S(z) = \sum_{i=0}^{m=4} P_i w_{i,4}(z) \quad (7)$$

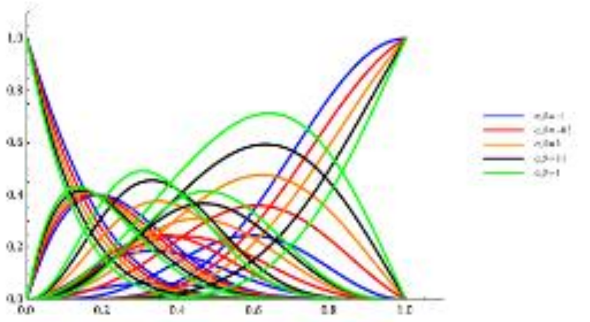

Figure 3: The Quartic GT-basis functions

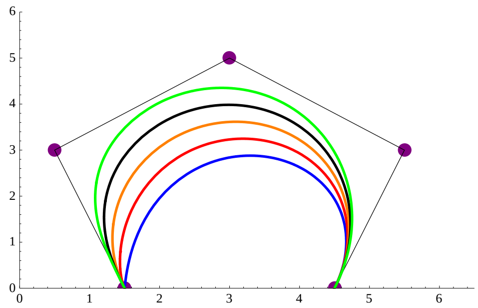

Figure 4: The Quartic GT-basis curves

Figure 3 and 4 shows all the graphs of Quartic GT-basis functions and curves. There are five shape parameters manipulated by alpha and beta [α, β], represented by the following colours: thick blue for [-1, -1], dotted red for [-0.5, -0.5], thick orange for [0, 0], dashed black for [0.5, 0.5], and thick green for [1, 1]. Five parameter pairs $[\alpha, \beta]$ were selected for analysis which are{ $[-1,-1]$, $[-0.5,-0.5]$, $[0,0]$, $[0.5,0.5]$, $[1,1]$. These values enable observation of curve deformation behaviour while maintaining the same control points, following the approach in Maqsood et al. (2020).

Data Acquisition And Discretization Process

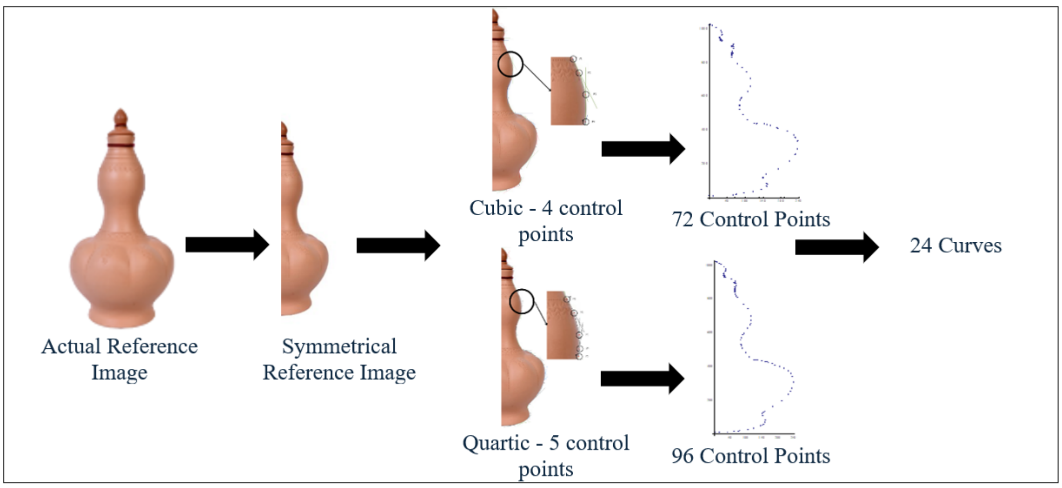

Figure 4: Data Discretization Process

Figure 4 is the diagram illustrates the digital modeling workflow for the *Labu Sayong*, moving from a physical object to a mathematical 3D profile. It begins with the Actual Reference Image, which is converted into a Symmetrical Reference Image to isolate the single-side silhouette. This profile is then evaluated using two methods: the Cubic model, which uses 4 control points per curve (72 total), and the Quartic model, which uses 5 control points per curve (96 total). Both methods result in a final silhouette of 24 curves. The control points is discretized into 24 distinct curves, with the numerical data organized systematically to facilitate the curve-fitting process was presented in Table 1 and 2.

Table 1: Discretized Control Points for Cubic GT-Bézier Profile Segments

Curve	**Control Points**	**Curve**	**Control Points**
1	P0={0,1022},P1={3.432,1022}, P2={7.807,1020},P3={20.31,1006},	13	P36={114.2,658.7},P37={106.4,628.1}, P38={90.93,592.3},P39={88.74,587.9},
2	P3={20.31,1006},P4={32.18,987.4}, P5={35.15,978.5},P6={35.15,964.6},	14	P39={88.74,587.9},P40={86.09,576.5}, P41={84.53,546.2},P42={84.53,524.5},
3	P6={35.15,964.6},P7={28.43,949}, P8={30.15,947.9},P9={29.99,939},	15	P42={84.53,524.5},P43:={93.43,492.1}, P44={107,462.3},P45={124.7,440.6},
4	P9={29.99,939},P10={31.09,938.5}, P11={32.81,937.1},P12={32.65,933.2},	16	P45={124.7,440.6},P46={131.6,440.4}, P47={153.7,435.6},P48={160.2,431.2},
5	P12={32.65,933.2},P13={32.49,929.8}, P14={35.78,927.7},P15={67.03,908.4},	17	P48={160.2,431.2},P49={171.1,427}, P50={188.6,412.7},P51={189.7,410.4},
6	P15={67.03,908.4},P16={67.03,899.8}, P17={64.37,898.1},P18={62.18,898.2},	18	P51={189.7,410.4},P52={217.7,393.5}, P53={234.4,371.7},P54={240,358.1},
7	P18={62.18,898.2},P19={62.03,896.3}, P20={63.9,895.1},P21={67.65,893.4},	19	P54={240,358.1},P55={246.4,335.4}, P56={246.4,289},P57={239.5,257},
8	P21={67.65,893.4},P22={67.81,882}, P23={63.74,863.7},P24={62.81,858.4},	20	P57={239.5,257},P58={223,217.9}, P59={191.9,172.1},P60={158,137.1},
9	P24={62.81,858.4},P25={65.62,857.7}, P26={65.62,851.8},P27={63.74,851.8},	21	P60={158,137.1},P61={149.5,123.1}, P62={149.8,116.5},P63={159.8,84.47},
10	P27={63.74,851.8},P28={64.37,845.9}, P29={63.12,844.3},P30={61.56,844.3},	22	P63={159.8,84.47},P64={161.1,80.09}, P65={159.5,67.75},P66={145.5,49.31},
11	P30={61.56,844.3},P31={62.96,832}, P32={78.43,795.2},P33={91.71,768.8},	23	P66={145.5,49.31},P67={122.3,35.56}, P68={96.24,26.03},P69={75.46,19.94},
12	P33={91.71,768.8},P34={103.3,744.8}, P35={114.1,706.7},P36={114.2,658.7},	24	P69={75.46,19.94},P70={66.56,16.34}, P71={10.62,12.59},P72={0,12.44},

Table 2: Discretized Control Points for Quartic GT-Bézier Profile Segments

Curve	**Control Points**	**Curve**	**Control Points**
1	P0={0,1022},P1={4.242,1022}, P2={8.485,1021},P3={15.3,1013}, P4={20.76,1007},	13	P48={114.2,658.4},P49={112.7,649.6}, P50={105.5,628.1},P51={94.09,599}, P52={88.79,588.5},
2	P4={20.76,1007},P5={30.61,991.6}, P6={36.52,977.8},P7={36.52,969.5}, P8={35,964.5},	14	P52={88.79,588.5},P53={85.15,571.7}, P54={83.33,556.6},P55={83.94,534}, P56={84.55,524.9},
3	P8={35,964.5},P9={30.3,951.3}, P10={29.09,947.9},P11={30.61,947.9}, P12={30.3,939.3}	15	P56={84.55,524.9},P57={88.48,509.5}, P58={98.48,482},P59={109.8,459.8}, P60={124.1,441.1},

4	P12={30.3,939.3},P13={31.52,938.7}, P14={32.73,937.9},P15={32.73,936}, P16={32.58,933.4},	16	P60={124.1,441.1},P61={129.8,440.8}, P62={135,440.2},P63={149.2,435.5}, P64={159.8,430.7},
5	P16={32.58,933.4},P17={32.73,928.7}, P18={33.94,928.5},P19={53.94,918.2}, P20={65.91,908.5},	17	P64={159.8,430.7},P65={164.1,429.5}, P66={168.8,427.3},P67={182.7,417.8}, P68={190.3,410.2},
6	P20={65.91,908.5},P21={67.12,906.6}, P22={67.12,901.1},P23={65.61,899.3}, P24={62.42,898.1},	18	P68={190.3,410.2},P69={205.2,401}, P70={218,389.9},P71={232.3,374.2}, P72={239.8,358.4},
7	P24={62.42,898.1},P25={62.58,895.8}, P26={63.79,896.1},P27={66.06,894.5}, P28={67.58,893.5},	19	P72={239.8,358.4},P73={245.2,341.3}, P74={248.6,308.7},P75={243.3,274.3}, P76={239.5,256.7},
8	P28={67.58,893.5},P29={67.58,880.4}, P30={65.61,872.2},P31={64.85,870.1}, P32={62.58,858.5},	20	P76={239.5,256.7},P77={232.1,236.3}, P78={211.2,197.5},P79={183.2,163.4}, P80={157.6,137.8},
9	P32={62.58,858.5},P33={64.7,858.2}, P34={66.36,856.6},P35={66.21,851.6}, P36={64.85,851.9},	21	P80={157.6,137.8},P81={154.4,132}, P82={150.5,121.7},P83={151.8,110.4}, P84={160,85.06},
10	P36={64.85,851.9},P37={65.15,846}, P38={65.15,844.8},P39={63.94,843.8} ,P40={62.12,843.8},	22	P84={160,85.06},P85={159.7,71.58}, P86={154.8,60.97},P87={151.5,54.76}, P88={145.3,49.76},
11	P40={62.12,843.8},P41={64.85,830.1}, P42={68.94,819.2},P43={73.03,809.9}, P44={91.82,769},	23	P88={145.3,49.76},P89={124.4,35.36}, P90={105.9,28.39},P91={80.45,20.51}, P92={75.15,19.61},
12	P44={91.82,769},P45={105.6,742.2}, P46={115.3,700.4},P47={115.5,673.7}, P48={114.2,658.4},	24	P92={75.15,19.61},P93={61.52,16.42}, P94={42.12,14},P95={15.15,12.18}, P96={0,12.44}

3d Reconstruction Using Rotational Sweep Surfaces

The 3D geometrical model of *Labu Sayong* is constructed by using the sweep surface technique, more precisely via the surface of revolution approach, which produces a continuous and smooth rotation surface by revolving a 2D profile curve along a defined axis (Foley et al., 1996). As the artifact has intrinsic axial symmetry, the GT-Bézier curve will be rotated along the y-axis to get the corresponding 3D representation. The surface that results can be mathematically formulated as follows:

Definition 4: Rotation Matrix and Surface Revolution

The revolution matrix for the y-axis as presented in equation (8):

$$T\,(w) \;=\begin{bmatrix} cos\,(w) & 0 & -sin\,(w) \\ 0 & 1 & 0 \\ sin\,(w) & 0 & cos\,(w) \end{bmatrix} \tag{8}$$

$$P(t,w) = P(t).T(w) \tag{9}$$

where:

$P\,(t,w)$: Surface Revolution

$P\,(t)$: Cross Section

$T\,(w)$: Matrix Revolution

This technique is commonly applied in the digital reconstruction of symmetrical artefacts such as pottery, vessels, and bottles (Razali et al., 2019).

ISSN No. 2454-6186 | DOI: 10.47772/IJRISS | Volume X Issue V May 2026

Evaluation Analysis

Computational Setup And Software Implementation

All modelling operations and numerical evaluations have been performed using Mathematica software, which is commonly recognised to have strong symbolic and numerical computational capabilities, which are suited to the formulation of curves and to the generation of surfaces in CAGD. Cubic and Quartic GT-Bézier models have been created on even grounds in regard to the computational setup to facilitate a fair comparison of performance.

Quantitative Performance Metrics

The factors were considered in the comparative analysis are the Root Mean Square Error (RMSE) for geometric accuracy, CPU processing time for computational efficiency, volumetric calculations for functional preservation and curvature profiles for smoothness.

Shape Fidelity and RMSE Analysis

Geometric accuracy is measured using the Root Mean Square Error (RMSE) between sampled reference points and model-generated surface coordinates. This metric quantifies the deviation between the actual artifact profile and the mathematical reconstruction.

$$\text{RMSE} = \sqrt{\frac{1}{n}\sum_{i=1}^{n}(\boldsymbol{x_1} - \boldsymbol{x_2})^2 + (\boldsymbol{y_1} - \boldsymbol{y_2})^2} \tag{10}$$

where:

x_1 coordinate from the actual

x_2 coordinate from the approximated

y_1 coordinate from the actual

y_2 coordinate from the approximated

Computational Efficiency (CPU Execution Time)

To determine the efficiency of computations, the internal timing mechanism of Mathematica was used to measure the CPU execution time. This study uses empirical values, which are the results of the modelling process directly and without any estimated and simulated performance figures. The calculations were done on an Intel Core i7 processor using a Windows based system with Mathematica and with an 16 GB RAM. This is in line with the benchmarking criteria in studies with CAGD-based modelling.

Volumetric Quantification for Functional Preservation

The functional capacity of the *Labu Sayong* is evaluated by treating the 2D profile curve as a surface of revolution. Since the pottery possesses intrinsic axial symmetry, the 3D model is generated by revolving the profile along the y-axis. Calculating the total internal volume is a critical metric for preservation, as it ensures the mathematical model is a functional representation of the physical vessel. Using the Theorem of Pappus-Guldinus, the volume (V) of a solid generated by revolving a parametric curve $S(z) = \{\text{x}(\text{z}), \text{y}(\text{z})\}$ about the y-axis is calculated by integrating the cross-sectional area along the height of the vessel. The formula is defined as:

$$\text{V} = \pi \int_0^1 [x(z)]^2 \left|\frac{dy}{dz}\right| dz \tag{11}$$

ISSN No. 2454-6186 | DOI: 10.47772/IJRISS | Volume X Issue V May 2026

Curvature Assessment (κ) for Surface Smoothness

In this study, curvature (κ) is utilized as a fundamental geometric diagnostic to evaluate the smoothness and organic fairness of the *Labu Sayong*'s reconstructed profile. For a parametric GT-Bézier $S(z) = \{x(z), y(z)\}$, the curvature κ is calculated using the first and second derivatives of the coordinate functions:

$$\kappa(z) = \frac{|x'(z)y''(z) - y'(z)x''(z)|}{(x'(z)^2 + y'(z)^2)^{3/2}} \tag{12}$$

RESULTS AND DISCUSSION

Results of modeling the *Labu Sayong* object using Cubic and Quartic GT-Bézier curves are presented in this section, along with a quantitative performance evaluation based on the Root Mean Square Error (RMSE) for geometric accuracy, CPU processing time for computational efficiency, volumetric calculations for functional preservation and curvature profiles for smoothness.

Analysis Of 2D Profile Curve Construction

The reference model of Labu Sayong was then discrete to define the control points of the 24 curve segments of the profile along the Cubic and Quartic GT-Bézier curves as display in Table 1 and 2. A respective GT-Bézier curve was fitted to each segment such that the overall geometry of the artefact could be best defined. The influence of different shape parameters on the curve geometry is given in Table 3, increased values yield a tighter curvature and more pronounced transitions along the curve segments. Qualitative visual inspection allows one to conclude from this result that the Cubic GT-Bézier curve reflects smoother continuity and more mild transitions at the junctions between adjacent segments in comparison with the Quartic formulation These observations indicate that the Cubic curve possesses a superior capability for preserving geometric smoothness and visual coherence in the artifact's overall profile.

Table 3: The varying shape parameter of 2D profile curves *Labu Sayong*

$[\alpha, \beta]$	$[-1, -1]$	$[-0.5, -0.5]$	$[0, 0]$	$[0.5, 0.5]$	$[1, 1]$
Cubic	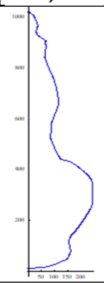	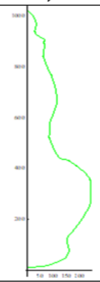		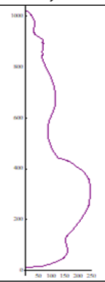	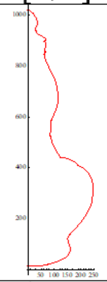
Quartic	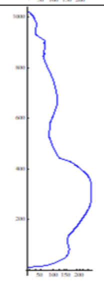	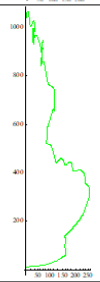	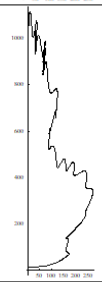	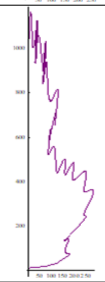	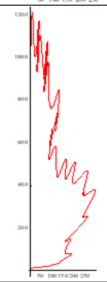

Evaluation Of Generated 3D Surfaces

The corresponding 3D models were generated by revolving the 2D profile curves through a full 360° rotation about the y-axis, employing the sweep surface method. This is represented in Table 4, which shows the effects of the chosen shape parameters on the geometry of the resulting surfaces. The Cubic GT-Bézier curve presents a smoother and more visually continuous 3D surface, while the Quartic model exhibits regions of sharper curvature and localized surface distortion. These observations suggest that an increase in curve order cannot

ISSN No. 2454-6186 | DOI: 10.47772/IJRISS | Volume X Issue V May 2026

unconditionally ensure geometrically smoother results and that an appropriate choice of curve formulation might always be necessary, depending on the actual balance between smoothness in the surface and precision in the structure.

Table 4: The varying shape parameter of 3D surface revolution *Labu Sayong*

$[\alpha,\beta]$	$[-1,-1]$	$[-0.5,-0.5]$	$[0,0]$	$[0.5,0.5]$	$[1,1]$
Cubic					
Quartic					

Comparative Analysis Of Geometric Accuracy

Geometric accuracy was quantitatively assessed using Root Mean Square Error (RMSE) against 345 ground-truth coordinates. The Cubic GT-Bézier curve achieved the highest geometric fidelity, reaching its lowest average RMSE of 1.33759 at shape parameter [1, 1]. In the error distribution graph in Figure 6, this configuration is represented by the red line, which consistently maintains the lowest position across nearly all 24 curve segments, indicating minimal deviation from the ground-truth coordinates. In contrast, the Quartic model exhibited significantly higher geometric errors, with deviations escalating up to 27.2486 under various parameter settings. Within the Quartic error graph, the blue line represents the shape parameter setting [-1, -1], which yielded the model's lowest average RMSE of 1.67039. While this blue line represents the best performance for the higher-order formulation, it still fails to match the precision of the Cubic model. Ultimately, the RMSE data validates that the Cubic formulation provides a more accurate and stable approximation of the artifact's silhouette than the higher-order Quartic model.

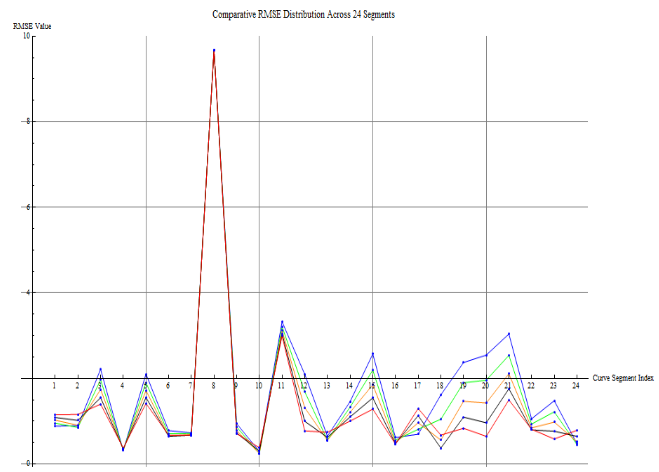

$\alpha,\beta = -1\ (Blue), \alpha,\beta = -0.5\ (Green),$
$\alpha,\beta = 0(Orrange), \alpha,\beta = 0.5(Black), \alpha,\beta = 1(Red)$

Figure 6: RMSE for Cubic GT-Bézier Models

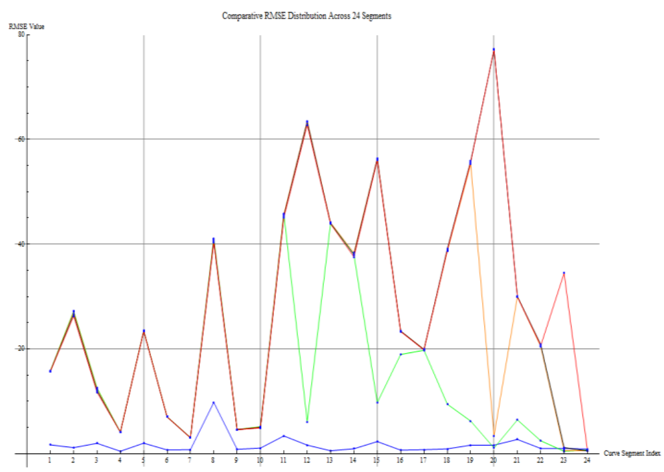

$\alpha,\beta = -1\ (Blue), \alpha,\beta = -0.5\ (Green),$
$\alpha,\beta = 0(Orrange), \alpha,\beta = 0.5(Black), \alpha,\beta = 1(Red)$

Figure 7: RMSE for Quartic GT-Bézier Models

ISSN No. 2454-6186 | DOI: 10.47772/IJRISS | Volume X Issue V May 2026

DISCUSSION OF COMPUTATIONAL OVERHEAD AND SCALABILITY

The analysis of computational efficiency highlights a significant disparity in processing requirements, with the Cubic model requiring an average CPU time of 96.78 seconds compared to 151.36 seconds for the Quartic model. This 36% increase in computational overhead for the Quartic formulation is due to the management of 96 control points as opposed to the 72 used in the Cubic model, alongside the increased complexity of higher-order basis functions. These findings reinforce that increasing model complexity may not yield proportional benefits in accuracy, suggesting that lower-order GT-Bézier curves offer better scalability for digital preservation.

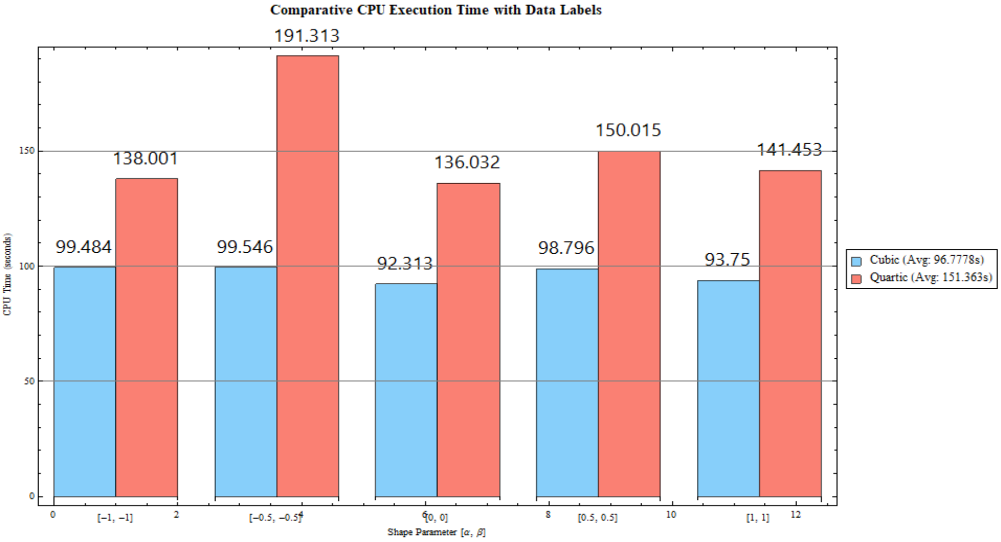

Figure 8: Comparative Computational Efficiency and CPU Execution Time Analysis

Volumetric Assessment And Functional Preservation

Volumetric quantification serves to validate that the mathematical models act as accurate functional representations of the physical artifact. By treating the profile as a surface of revolution and applying the Theorem of Pappus-Guldinus, the total internal capacity was detailed for both Cubic and Quartic models. Comparative analysis reveals that the Cubic formulation achieves significantly higher efficiency in volumetric calculation while maintaining the vessel's traditional proportions. These results ensure that digital preservation efforts successfully replicate the functional utility of the traditional *Labu Sayong* water vessel.

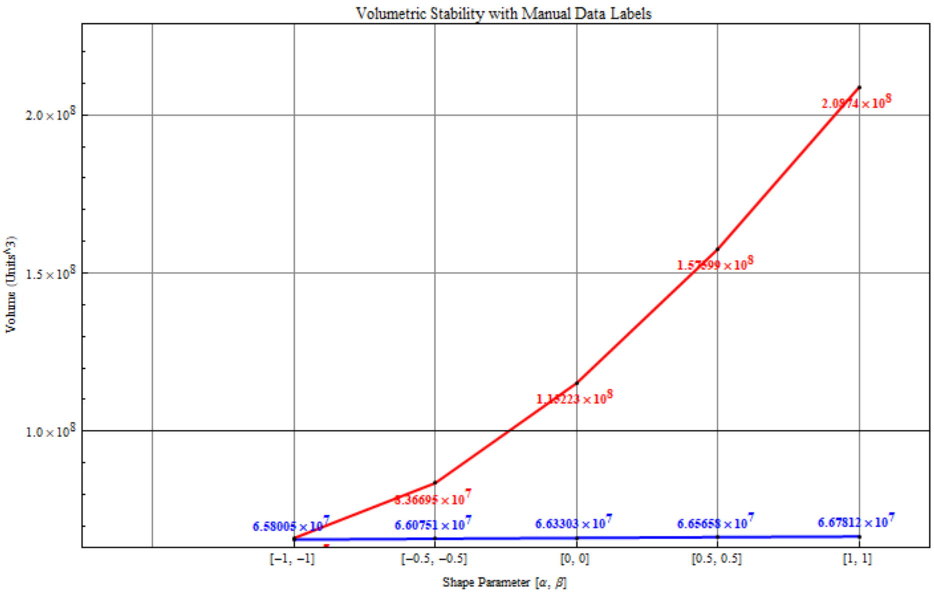

Figure 9: Volumetric Quantification of the *Labu Sayong* Profile

Curvature Analysis And Surface Smoothness

Curvature plots (κ) provide an essential diagnostic of the organic flow and geometric fairness of the reconstructed profile. As illustrated in Figures 8 and 9 the (κ) values for the 24 segmented curves were plotted across multiple shape parameter settings to evaluate surface stability. The results confirm that the Cubic GT-Bézier curve maintains a stable curvature distribution, ensuring visual coherence and seamless transitions between the vessel's concave and convex regions. In contrast, the Quartic GT-Bezier model exhibited localized ripple distortions and curvature fluctuations, which negatively impact the aesthetic integrity and smoothness of the 3D surface.

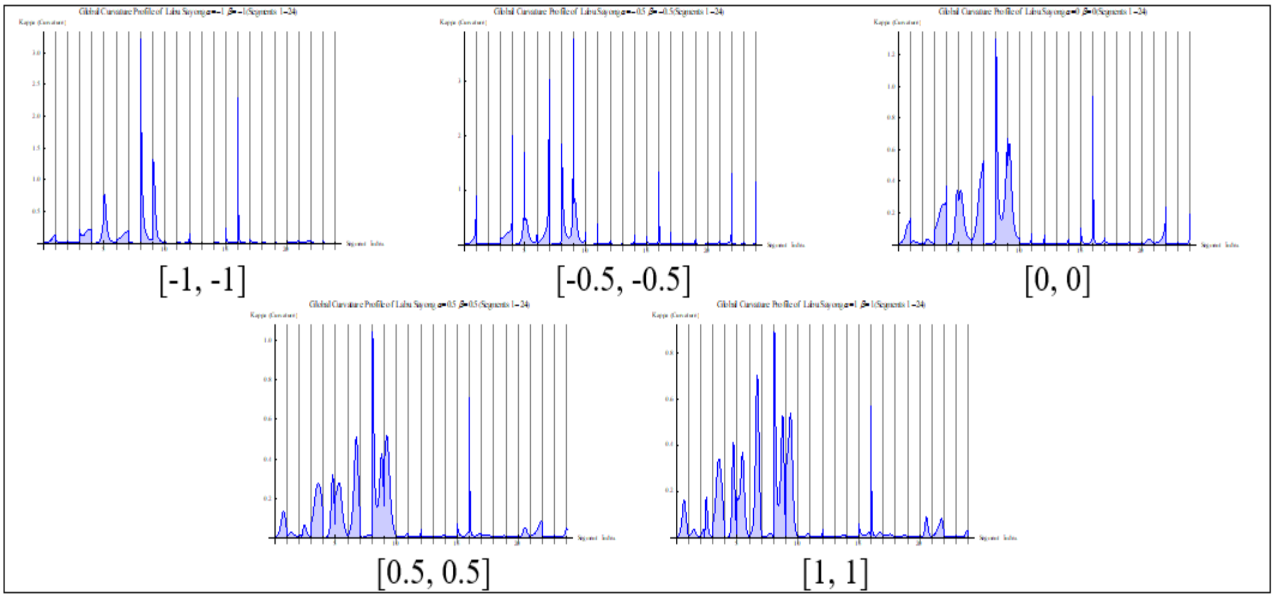

Figure 10: Global Curvature Cubic GT-Bezier Profile of *Labu Sayong*

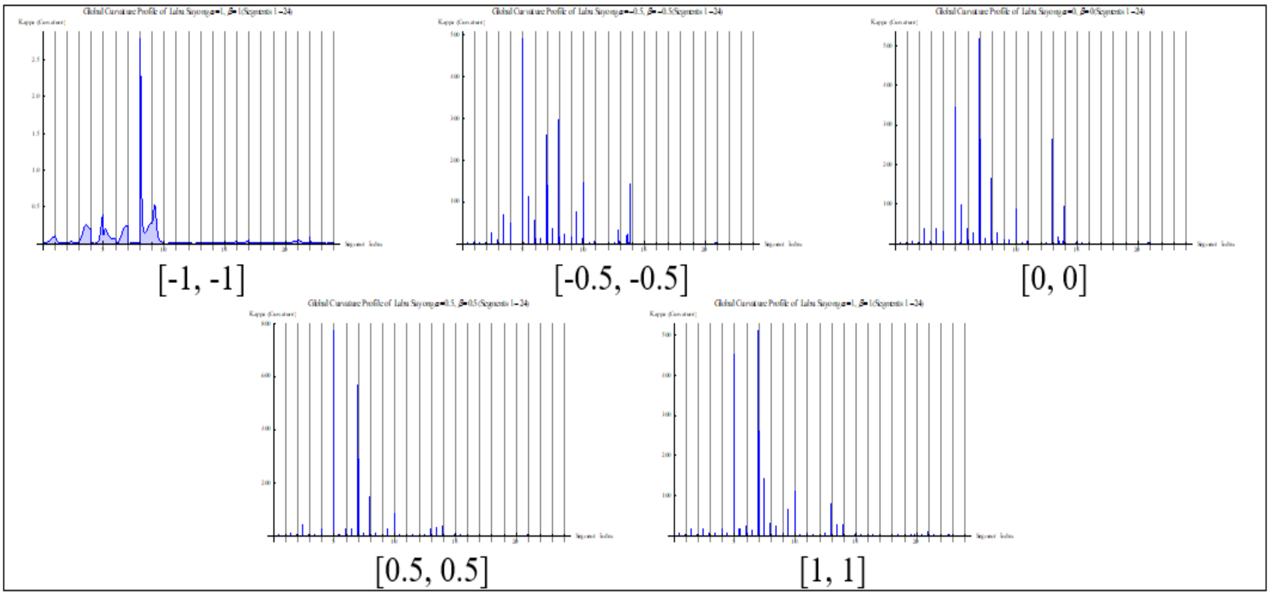

Figure 11: Global Curvature Quartic GT-Bezier Profile of *Labu Sayong*

CONCLUSION AND FUTURE WORK

This research presented a systematic comparative study of Cubic and Quartic GT-Bézier curves for the 3D reconstruction of the traditional *Labu Sayong* using the rotational sweep surface method. The comparative evaluation demonstrate that the Cubic GT-Bézier formulation is the optimal choice for the digital preservation of *Labu Sayong*. Results consistently indicate that the Cubic model strikes a superior balance between geometric fidelity, surface smoothness, and computational efficiency compared to its Quartic counterpart. Specifically, the Cubic model yielded the lowest geometric average error (RMSE 1.33759) and required significantly less processing time in average of 96.78 seconds, whereas the Quartic model exhibited larger deviations and consumed approximately 36% more CPU time due to added mathematical complexity. From a functional standpoint, the volumetric quantification confirms that the mathematical model serves as a valid representation of the physical vessel, with the Cubic model achieving greater efficiency in volumetric calculation while successfully preserving the artifact's essential geometry and functional capacity. Furthermore, curvature analysis confirms that the Cubic formulation maintains a stable organic flow, avoiding the localized ripple distortions and fluctuations observed in the Quartic model. These findings uphold the principle that for axially symmetric artifacts, increasing the curve order does not necessarily guarantee improved fitting quality but instead introduces unnecessary computational overhead and potential surface instability.

Ultimately, this study proves that a third-order formulation is mathematically sufficient to capture the intricate proportions of rotationally symmetric cultural artifacts with high precision and smoothness. These findings provide critical guidelines for curve selection in CAGD applications, emphasizing that an optimal balance between geometric control and processing efficiency is essential. Future work should focus on automating control point extraction and extending this evaluation framework to even higher-order formulations, such as Quintic or rational GT-Bézier curves, to further refine the digital preservation of cultural heritage.

ACKNOWLEDGMENTS

The authors would like to express their sincere appreciation to the Faculty of Computer and Mathematical Sciences, Universiti Teknologi MARA Cawangan Terengganu, for providing the facilities, technical resources, and academic support necessary to complete this research.

REFERENCES

1. Abd Aziz M.Z. & Samsudin A. 2025. Echo of Earth: The Labu Sayong Heritage Centre. National EngiTech Digest 1(1): 32–45.
2. Arifin A. 2015. Traditional Malay pottery of Kuala Kangsar: Its history and development. Kajian Malaysia 33(Supplement 2): 113–133.
3. Farin G. 2002. Curves and Surfaces for CAGD: A Practical Guide (5th ed.). Morgan Kaufmann.
4. Foley J.D., van Dam A., Feiner S.K. & Hughes J.F. 1996. Computer Graphics: Principles and Practice (2nd ed.). Addison-Wesley.
5. Hamdzun Haron N.A.Y., Yusof S., Haron S., Basir A., Yusof A.S., Zulkifli M. & Alias J. 2018. The fineness of design motif and pattern of Labu Sayong. International Journal of Mechanical Engineering and Technology 9(7): 1494–1502.
6. Hu G., Ji X. & Guo L. 2014. Quartic generalized Bézier surfaces with multiple shape parameters and its continuity conditions. Nongye Jixie Xuebao / Transactions of the Chinese Society for Agricultural Machinery 45(2): 123–130.
7. Mahmoud W.M., Soliman M.A. & Mohamed E.M. 2023. Investigation on isotropic Bézier sweeping surface (IBSS) with Bishop frame. Mathematics and Statistics 11(4): 857–871.
8. Maqsood S., Abbas M., Hu G., Ramli A.L.A. & Miura K.T. 2020. A novel generalization of trigonometric Bézier curve and surface with shape parameters and its applications. Mathematical Problems in Engineering 2020: 4036434. https://doi.org/10.1155/2020/4036434
9. Meng W., Xin S., Zhao J. & He Y. 2021. A variational framework for computing geodesic paths on sweep surfaces. Computer-Aided Design 132: 102965. https://doi.org/10.1016/j.cad.2021.102965
10. Qin X., Hu G., Yang Y. & Wei G. 2016. The fairing and G1 continuity of quartic C-Bézier curves. Mathematical Methods in the Applied Sciences 39(10): 2613–2624. https://doi.org/10.1002/mma.3713
11. Razali N.K., Nor-al-Din S.M., Mohamad Sukri N., Adenan M.A. & Abdul Azib M.H. 2019. Bézier and trigonometric Bézier with a shape parameter curve in designing 3-dimensional objects using rotational sweep surface method. International Journal of Advanced Trends in Computer Science and Engineering 8(1.5): 35–39. https://doi.org/10.30534/ijatcse/2019/0881.52019

12. Remondino F. & Rizzi A. 2010. Reality-based 3D documentation of natural and cultural heritage sites—Techniques, problems, and examples. Applied Geomatics 2(3): 85–100.
13. Sederberg T.W. 2012. Computer-Aided Geometric Design Course Notes. Brigham Young University.
14. Sun X., Qiao Y. & Li H. 2019. Subdivision algorithm of quartic λ-Bézier curves with shape parameters. In Proceedings of the 2019 IEEE 4th International Conference on Image, Vision and Computing (ICIVC), pp. 562–566. IEEE. https://doi.org/10.1109/ICIVC47709.2019.8981138
15. Yu Y.Y., Li X. & Ji Y. 2024. On self-intersections of cubic Bézier curves. Mathematics 12(3): 421. https://doi.org/10.3390/math12030421
16. Zhang R., Yang J. & Li R. 2009. Investigation on parametric design of centrifugal pump blade. Paiguan Jixie / Drainage and Irrigation Machinery 27(4): 23–28.